

Correlated states of a triangular net of coupled quantum wires: Implications for the phase diagram of marginally twisted bilayer graphene

Chuan Chen,^{1,2} A. H. Castro Neto,^{1,3} and Vitor M. Pereira^{1,3,*}

¹*Centre for Advanced 2D Materials and Graphene Research Centre,
National University of Singapore, Singapore 117546*

²*Max-Planck Institute for the Physics of Complex Systems, 01187 Dresden, Germany*

³*Department of Physics, National University of Singapore, Singapore 117542*

(Dated: April 29, 2020)

We explore in detail the electronic phases of a system consisting of three non-colinear arrays of coupled quantum wires, each rotated 120 degrees with respect to the next. A perturbative renormalization-group analysis reveals that multiple correlated states can be stabilized: a s -wave or $d \pm id$ superconductor, a charge density wave insulator, a two-dimensional Fermi liquid, and a 2D Luttinger liquid (also known as smectic metal or sliding Luttinger liquid). The model provides an effective description of electronic interactions in small-angle twisted bilayer graphene and we discuss its implications in relation to the recent observation of correlated and superconducting ground states near commensurate densities in magic-angle twisted samples, as well as the “strange metal” behavior at finite temperatures as a natural outcome of the 2D Luttinger liquid phase.

I. INTRODUCTION

The low-energy physics of interacting fermions in one dimension (1D) is determined by collective spin and charge density excitations that define what is known as Luttinger liquid (LL) behavior^{1–3}. Soon after high-temperature superconductivity was discovered in cuprate oxides⁴, it was proposed that the charges added upon doping a Mott insulator could end up distributed in stripes^{5–9}. This led Anderson *et al.* to suggest that confined fermionic excitations in such presumed LL arrays (the stripes) could explain the non-Fermi-liquid nature of cuprates’ “normal” state¹⁰. Since then, theoretical investigation has assessed whether LL behavior can emerge in higher dimensions, especially in 2D^{10–15}, the natural route to that having been to study systems of coupled LLs in different guises. It is now known, for example, that, in an array of parallel LLs, marginal inter-wire density-density and current-current interactions lead to strong transverse charge-density fluctuations at incommensurate wave vectors which can frustrate electron crystallization and indeed stabilize a LL state, commonly designated “smectic metal” or “sliding Luttinger liquid” state^{12–15}. However, previous work has been limited to exploring consequences of couplings among either one or two perpendicularly crossed arrays, without ever considering LLs interlinked in the form of a triangular net, possibly for lack of a realistic representative system.

The recent discovery of strongly correlated physics in marginally twisted bilayer graphene (MTBG) near the magic angle $\theta \approx 1.1^\circ$ ^{16,17} set off a flurry of interest in the origin of the observed insulating and superconducting (SC) phases. (For the purposes of this work, MTBG refers to bilayers twisted by $\sim 1^\circ$ or less, including the first magic angle.) It had been previously suggested that, at magic angles, the quasi-flatness of the electronic bands closest to the undoped Fermi level could promote electronic instabilities^{18–21}. The development of effective

tight-binding models for those bands^{22–25} enabled, on the one hand, predictions of possible broken symmetries arising from weak-coupling mechanisms, such as Fermi surface nesting or enhanced density of states^{24,26–29}; on the other hand, it revealed trilobed Wannier functions centered at the AB/BA positions^{23–25}, which has in turn motivated strong-coupling perspectives based on extended and non-conventional Hubbard-type interactions^{30–32}. Electronic interactions are an undisputed factor given that the ratio of the local Coulomb integral to bandwidth is estimated in the range $U/w \sim 5–10$ ²³. The extremely large Moiré unit cells involved ($\sim 172 \text{ nm}^2$, about 100 times those of canonical Mott-insulators like cuprates) has also prompted the suggestion that the insulating phase can be a Wigner crystal, consistently with the extremely low densities, and the emergence of SC a result of its melting^{33,34}.

Evidence accumulated from recent experiments and theoretical work motivates a different perspective over the effective electronic model governing correlations in MTBG, which we develop in this paper. We note, first, that, by allowing more than the minimum two orbitals²⁴ per Moiré unit cell, Carr *et al.* have recently shown that the weight of the Bloch states belonging to the flat-band sector is overwhelmingly distributed among Wannier functions situated at the AA positions *and* at the AB/BA *domain boundaries*³⁵. Second, it is well known that, in the presence of perpendicular electrical fields, AB-BA domain boundaries host protected helical modes^{36–40}. MTBG accommodates well defined, intrinsic, and periodically alternating AB/BA regions²¹ whose network of boundaries was shown to likewise support the propagation of such confined states^{41–43}. Moreover, since AB is favored against AA stacking, a considerable atomic relaxation within the Moiré unit cell maximizes the AB/BA regions, leaving sharply defined, atomic-scale domain boundaries^{44–49}. Crucially, there is now unequivocal spectroscopic^{44,50–53} and transport^{50,54–56} evidence of the reality of this network of 1D modes in MTBG,

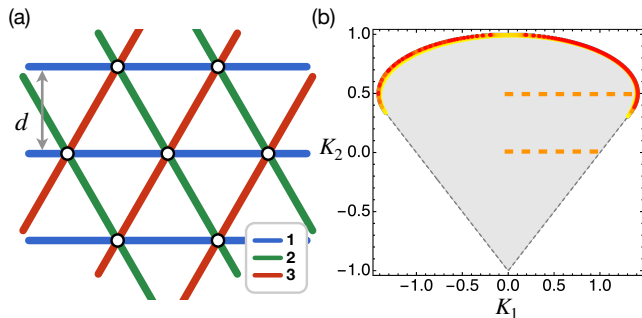


FIG. 1. (a) Schematic of the local net spanned by the three coupled arrays of quantum wires, labeled $\{1, 2, 3\}$. One *array* consists of a set of parallel, identically colored wires. The superposition of the three arrays reproduces the net of AB-BA domain boundaries in MTBG. (b) Domain of stability. The array’s effective Luttinger parameter, $\kappa(k_{\perp})$, is positive in the shaded domain for all $k \in (-\pi/d, \pi/d)$. The LL phase exists *only* in the red-to-yellow region surrounding the upper boundary. Dashed lines indicate the cuts chosen to generate the phase diagrams in Fig. 2.

including in single-gated devices.

There are additional hints that warrant a description in terms of such “network of linked quantum wires” to describe the observed correlated behavior: the confinement of electrons to 1D naturally boosts correlations; a phase diagram similar to that of magic-angle samples arises at other twist angles under pressure⁵⁷, in line with the expectation that an inter-layer coupling enhanced by pressure would amplify the lattice relaxation, in turn defining sharp domain boundaries and the emergence of the wire network for more generic twists^{54–56}.

All the above aspects and observations call for an investigation of the implications of a coupled-wire description of the low-energy physics of MTBG. Wu *et al.* have recently advanced arguments to justify the insulating and SC phases in such a scenario, but only considering coupling at the wire intersections and spin isotropic interactions within each wire⁵⁸. By generalizing to MTBG the approach developed to study sliding LL phases, we scrutinize not only the competition among SC and charge-density wave (CDW) states, but also the emergence of Fermi liquid (FL) and sliding LL phases that, stabilized by inter-wire interactions, might explain the experimental progression of MTBG from an insulator to SC to a metal as density deviates from commensurate fillings. The SC order parameter acquires either s or $d \pm id$ symmetry, depending on the Josephson coupling at the wire crossings. Moreover, it suggests that these correlated phases could also happen in “marginally” ($\theta \ll 1^\circ$) twisted bilayer graphene. Finally, we emphasize that, independently of its direct relevance to MTBG, this work reports the first detailed study of coupled quantum wires and sliding LL phases in a triangular net geometry.

II. COUPLED-WIRE MODEL

A. Interconnected Luttinger liquid array

Mirroring the experimental network of AB-BA boundaries, we consider three families of quantum wires, each family consisting of an array of parallel wires depicted by the same color in Fig. 1(a). Although each link in MTBG supports two helical channels per spin along the forward and backward direction, we study the simplified case of a single mode per wire, which should capture the essential physics at play. Each independent wire is a LL whose excitations are best described in the boson formalism by a separated spin (s) and charge (c) Hamiltonian (see Appendix for the convention of bosonization)^{1–3},

$$H = \sum_{\alpha=c,s} \int dx \frac{v_{\alpha}}{2} \left[\frac{1}{K_{\alpha}} (\partial_x \theta_{\alpha})^2 + K_{\alpha} (\partial_x \phi_{\alpha})^2 \right], \quad (1)$$

where $\theta_{\alpha}(x)$ and $\phi_{\alpha}(x)$ are the conventional phase-field operators, $K_{c/s}$ is the (inverse) charge/spin Luttinger parameter ($K_c \geq 1$ for repulsive/attractive interactions), and v_{α} defines the velocity of each excitation. Spin back-scattering adds the term $2g_s/(2\pi\alpha)^2 \int dx \cos(2\sqrt{2}\pi\phi_s)$, where α is the (length) cutoff of the theory, to Hamiltonian (1), leading to a sine-Gordon-like action and spin couplings that flow according to the equations²

$$\frac{dg_s}{dl} = 2\left(1 - \frac{1}{K_s}\right)g_s, \quad \frac{dK_s}{dl} = \frac{g_s^2}{2\pi^2 v_s^2}. \quad (2)$$

As a result, when there is a spin gap, $K_s \rightarrow \infty$.

To describe each periodic array of parallel wires separated by d as in Fig. 1, one must include the long-wavelength (charge) density-density and current-current interactions among wires in the fixed-point Hamiltonian, as first noted by Emery *et al.*¹². It can then be shown that the charge part of the action reads, in Fourier space,

$$S = \sum_q \frac{v(k_{\perp})k^2}{2} \left[\frac{|\theta_{c,q}|^2}{\kappa(k_{\perp})} + \kappa(k_{\perp})|\phi_{c,q}|^2 \right] + i\omega_n k \phi_{c,q}^* \theta_{c,q}, \quad (3)$$

where $q \equiv (\omega_n, k, k_{\perp})$ and k/k_{\perp} is the momentum along/perpendicular to the wires^{12–14}. The spin part, for θ_s and ϕ_s , is obtained by replacing $[v(k_{\perp}), \kappa(k_{\perp})] \rightarrow [v_s, K_s]$. Direct comparison with Eq. (1) shows that an array of LLs effectively behaves as a LL, the net effect of the inter-wire coupling being a Luttinger parameter κ that is now a $2\pi/d$ -periodic function of k_{\perp} . This periodicity justifies a Fourier expansion,

$$\kappa(k_{\perp}) = K_0[1 + K_1 \cos(k_{\perp}d) + K_2 \cos(2k_{\perp}d) + \dots], \quad (4)$$

which we shall use below with $K_{0,1,2}$ as free parameters^{13–15}.

Each of the three LL arrays depicted in Fig. 1 is assigned a (superscript) label $j \in \{1, 2, 3\}$. Within each array j , we consider the single-electron hopping (t_{\perp}) between nearest-neighboring wires, as well as inter-wire

CDW (\mathcal{V}_n) and SC (\mathcal{J}_n) singlet interactions between n -th neighboring wires. These are described, respectively, by the *intra*-array, *inter*-wire couplings

$$\mathcal{H}_h^j = t_\perp \sum_{l,\sigma} \sum_{\nu=\pm 1} \psi_{l,\nu,\sigma}^{j\dagger} \psi_{l+1,\nu,\sigma}^j + \text{H. c.}, \quad (5a)$$

$$\mathcal{H}_{c,n}^j = \mathcal{V}_n \sum_{l,\sigma,\sigma'} \psi_{l,\nu,\sigma}^{j\dagger} \psi_{l,-\nu,\sigma}^j \psi_{l+n,-\nu,\sigma'}^{j\dagger} \psi_{l+n,\nu,\sigma'}^j, \quad (5b)$$

$$\mathcal{H}_{sc,n}^j = \mathcal{J}_n \sum_{l,\mu,\nu} \psi_{l,\mu,\uparrow}^{j\dagger} \psi_{l,-\mu,\downarrow}^{j\dagger} \psi_{l+n,\nu,\downarrow}^j \psi_{l+n,-\nu,\uparrow}^j + \text{H. c.}, \quad (5c)$$

where $\psi_{l,\pm 1,\sigma}^i$ is the field operator for a right/left-moving electron of spin σ in the l -th wire of array i . The wires are also coupled at each intersection [white dots in Fig. 1(a)], requiring us to consider the additional *inter*-array hopping, CDW and SC interactions:

$$H_h^{i,j} = t \sum_{l,m,\sigma} \sum_{\mu,\nu} \psi_{l,\mu,\sigma}^{i\dagger} \psi_{m,\nu,\sigma}^j + \text{H. c.}, \quad (6a)$$

$$H_c^{i,j} = \mathcal{V}_0 \sum_{l,m} \sum_{\sigma,\sigma'} \sum_{\mu,\nu} \psi_{l,\mu,\sigma}^{i\dagger} \psi_{l,\mu,\sigma}^i \psi_{m,\nu,\sigma'}^{j\dagger} \psi_{m,\nu,\sigma'}^j, \quad (6b)$$

$$H_{sc}^{i,j} = \mathcal{J}_0 \sum_{l,m,\mu,\nu} \psi_{l,\mu,\uparrow}^{i\dagger} \psi_{l,-\mu,\downarrow}^{i\dagger} \psi_{m,\nu,\downarrow}^j \psi_{m,-\nu,\uparrow}^j + \text{H. c.} \quad (6c)$$

B. Renormalization group equations

Once all the couplings in Eqs. (5) and (6) are written in terms of the bosonic fields, we proceed by developing a perturbative renormalization group (RG) analysis. To the lowest order, the flow equations for the hopping (t , t_\perp), CDW (\mathcal{V}_n), and SC (\mathcal{J}_n) coupling parameters read:

$$\frac{d\mathcal{V}_n}{dl} = (2 - \delta_{n,0} - \frac{1}{K_s} - \Delta_{C,n})\mathcal{V}_n, \quad (7a)$$

$$\frac{d\mathcal{J}_n}{dl} = (2 - \delta_{n,0} - \frac{1}{K_s} - \Delta_{S,n})\mathcal{J}_n, \quad (7b)$$

$$\frac{dt_\perp}{dl} = \left[2 - \frac{1}{4}(K_s + \frac{1}{K_s}) - \frac{1}{4}(\Delta_{C,1} + \Delta_{S,1}) \right] t_\perp, \quad (7c)$$

$$\frac{dt}{dl} = \left[1 - \frac{1}{4}(K_s + \frac{1}{K_s}) - \frac{1}{4}(\Delta_{C,0} + \Delta_{S,0}) \right] t, \quad (7d)$$

where,

$$\Delta_{C,n} \equiv \int_{-\pi}^{\pi} \frac{dk}{2\pi} [1 - (1 - \delta_{n,0}) \cos(nk)] \frac{1}{\kappa(k/d)}, \quad (8a)$$

$$\Delta_{S,n} \equiv \int_{-\pi}^{\pi} \frac{dk}{2\pi} [1 - (1 - \delta_{n,0}) \cos(nk)] \kappa(k/d). \quad (8b)$$

It is physically reasonable to expect the intra-array couplings to decay rapidly so, henceforth, we only consider intra-array CDW and SC interactions up to second-neighbors. As for $\kappa(k_\perp)$, in line with Vishwanath and Carpentier¹³, we truncate its Fourier expansion at the

Coupling	$(0, K_-)$	$(K_-, 1/2)$	$(1/2, 1)$	$(1, K_+)$	(K_+, ∞)
intra-array (among parallel wires)					
\mathcal{V}_n (CDW)	–	–	✓	✓	✓
\mathcal{J}_n (SC)	–	–	✓	✓	✓
t_\perp (hop)	–	✓	✓	✓	–
inter-array (at wire crossings)					
\mathcal{V}_0 (CDW)	–	–	–	✓	✓
\mathcal{J}_0 (SC)	–	–	–	✓	✓
t (hop)	–	–	–	–	–

TABLE I. Relevance of each coupling for the different ranges of the spin Luttinger parameter (K_s) specified in the first row. The symbol ✓ means that a coupling *may* be relevant while “–” indicates it is *always* irrelevant within that interval of K_s . $K_- \equiv 3 - 2\sqrt{2} \simeq 0.17$, $K_+ \equiv 3 + 2\sqrt{2} \simeq 5.83$.

second order. Furthermore, in order to have a stable theory, $\kappa(k_\perp)$ must be positive for $k_\perp \in (-\pi/d, \pi/d)$, which constrains $K_0 > 0$ and (K_1, K_2) to the shaded domain shown in Fig. 1(b).

At this level of approximation, the RG equations (7) are independent. The relevancy of the different couplings can thus be immediately established and is summarized in Table I. Since κ is strictly positive, $\Delta_{C,0} + \Delta_{S,0} \geq 2$ which, according to Eq. (7d), implies that the single-electron hopping at the wire intersections (t) is, at most, marginal if $K_s = 1$ and $\kappa(k/d) = 1$ for all k ; it is otherwise irrelevant in nearly the whole phase space. This justifies considering t globally irrelevant and, accordingly, it will be ignored in the subsequent analysis. Similarly, one can see that $\Delta_{C,1} + \Delta_{S,1} \geq 2$ so that the intra-array hopping (t_\perp) may be relevant when $3 - 2\sqrt{2} \leq K_s \leq 3 + 2\sqrt{2}$. The CDW and SC couplings are relevant only if $K_s > 1/2$ in the intra-array case ($\mathcal{V}_{1,2}$ and $\mathcal{J}_{1,2}$), while the corresponding inter-array couplings (\mathcal{V}_0 and \mathcal{J}_0) are relevant for $K_s > 1$.

Up to this point, the spin Luttinger parameter K_s has been considered free; Table I thus covers the most general scenario in relation to the possible magnetic phases. However, addition of the spin backscattering term mentioned earlier to Eq. (1) makes K_s a running coupling, governed by the flow Eqs. (2). The solution where $K_s \rightarrow \infty$ corresponds to a spin-gapped state, in which case we find the single-electron hoppings t and t_\perp to be irrelevant (last column of Table I), in correspondence with previous calculations for a single array of coupled quantum wires¹². In contrast, if $K_s \rightarrow 0$ we have a spin gapless state and all the couplings considered here are irrelevant — the system consists of decoupled LLs.

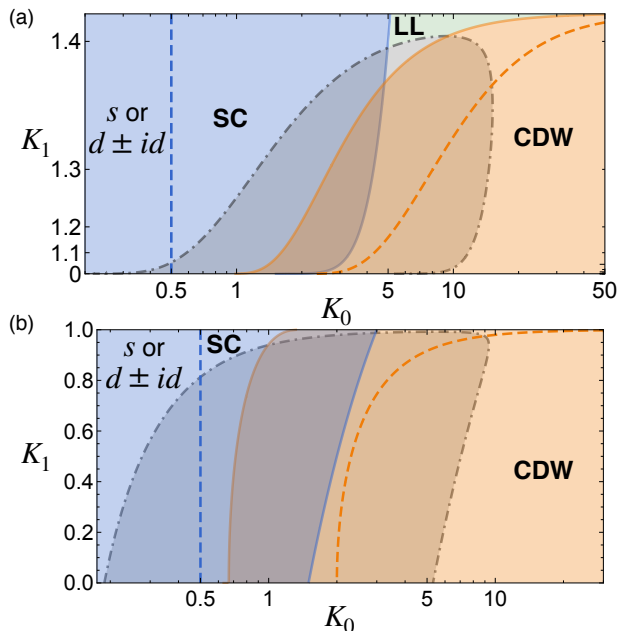


FIG. 2. Phase diagram along the horizontal cuts marked in Fig. 1 and for $K_s = 2$: (a) $K_2 = 0.5$, (b) $K_2 = 0$. The parameters K_0 and K_1 (axes) are the Fourier coefficients defined in Eq. (4). In the region above the solid-blue line, one of \mathcal{J}_1 or \mathcal{J}_2 is relevant (SC order). In the region below the solid-orange line, at least one of \mathcal{V}_1 and \mathcal{V}_2 is relevant (CDW order). The intra-array hopping (t_\perp) is relevant in the gray domain bounded by the dash-dotted line, implying that the system might be a Fermi liquid in this region. To the left of the blue-dashed line, the inter-array SC coupling is relevant, whereas the inter-array CDW coupling is relevant to the right of the orange-dashed line. The green area indicates a regime where all the couplings are irrelevant, corresponding to a 2D LL state. The main difference between (a) and (b) is the absence of the LL phase in the latter.

III. PHASE DIAGRAM AND ANALYSIS

A. Instability tendencies

While one may explore any range of K_s , we will now focus on $K_s = 2$. Table I shows that this falls in the regime where all couplings but t are relevant and, therefore, it is representative of the physical scenarios involving phase competition, as is the case of MTBG, either driven by inter- or intra-array interactions (or both). Figure 2 shows the phase diagram in two representative scenarios, defined by different magnitudes of the second harmonic in the Fourier expansion (4). Although K_0 is not strictly the Luttinger (charge) parameter of an individual wire, Eq. (3) implies it does represent the effective Luttinger parameter of an array behaving collectively as a LL¹². Therefore, $K_0 < 1$ signals an effectively attractive regime while $K_0 > 1$ describes repulsion. In this context, one qualitatively understands the fact that the SC phase (blue region) dominates in the small- K_0 portion of the

phase diagram, while the CDW eventually becomes the only relevant phase for large K_0 . In the crossover region $K_0 \sim 1$, the domains of relevancy for the CDW and SC orders overlap; in addition, the intra-array hopping is relevant as well in this case (gray region enclosed by the dot-dashed line) which, should the hopping become dominant over the CDW and SC instabilities, implies the existence of a 2D FL phase. This indicates that the transition between SC and CDW with increasing repulsion (increasing K_0) can occur either directly or via an intervening FL phase, depending on the magnitude of K_1 (which is a measure of the nearest-neighbor inter-wire coupling within an array). The precise outcome of this phase competition, or coexistence, depends on how the running of one coupling constant affects the others, whose analysis requires a perturbative RG calculation beyond first order, which is not in the scope of this paper.

When K_2 is finite, in addition to a FL, one finds that a LL phase is stabilized between the SC and CDW region close to the parameter-space boundary at $K_1 \rightarrow \sqrt{2}$. This is marked by the green area in Fig. 2(a) or the orange region in Fig. 1(b). Physically, the appearance of a LL phase in this case arises from the fact that K_2 promotes interaction between next-nearest-neighbor wires within an array, which is detrimental to the stability of the CDW. As first pointed out by Vishwanath and Carpentier¹³, when K_2 is included, near the (K_1, K_2) space boundary, the minimum of the $\kappa(k_\perp)$ is located at some *incommensurate* k_\perp and the value is close to zero, which indicate strong fluctuations of a transverse incommensurate CDW order [the density correlation $\langle \phi_{c,k,k_\perp}^* \phi_{c,k,k_\perp} \rangle \propto 1/\kappa(k_\perp)$]. The *incommensurate* CDW fluctuations then destroy the crystallization so that all couplings are irrelevant within that region. In contrast, for $K_2 = 0$, the most divergent transverse CDW is commensurate as $K_1 \rightarrow 1$; i.e., $1/\kappa(k_\perp) = 1/K_0[1 + \cos(k_\perp d)]$ diverges at $k_\perp = \pi/d$, so the next-nearest-neighbor intra-array CDW coupling will crystallize the system and there is no LL phase. Indeed, comparing Figs. 2(a) and 2(b), we see that a LL phase is stabilized at the expense of the CDW phase in the repulsive region ($K_0 > 1$), without much impact on the region of SC stability. At large K_0 , both intra-array (rightward off the solid orange line) and inter-array (rightward off the dashed orange line) CDW couplings are relevant — the electrons crystallize and an insulator ensues.

If $K_0 < 0.5$, the inter-array Josephson coupling is relevant. At each wire crossing, the phases of the three SC order parameters couple via

$$\propto \mathcal{J}_0 \sum_{i,j \in \{1,2,3\}} \cos(\varphi_{\mathbf{r}}^i - \varphi_{\mathbf{r}}^j). \quad (9)$$

Assuming that the intra-array SC coupling promotes uniform SC within each array, Eq. (9) indicates that the global SC phase depends on the sign of \mathcal{J}_0 : if $\mathcal{J}_0 < 0$, the Josephson coupling favors *s*-wave SC with all φ_i equal; but, if $\mathcal{J}_0 > 0$, that coupling is frustrated and will result in a $2\pi/3$ difference between the phase of the SC

order parameter of one array (j) with respect to the next ($j+1$). This originates a $d \pm id$ SC symmetry. A similar conclusion has been drawn by Wu *et al.* who have further considered triplet pairing and discuss the additional possibility of $p \pm ip$ symmetry⁵⁸.

B. Commensurability

In a conventional (i.e., single) LL problem, the proximity to commensurate electron densities is described by considering the Umklapp process within each wire² which, in the notation of Eq. (1), has the form

$$\frac{g_U}{(2\pi\alpha)^2} \int dx \cos[2\sqrt{2\pi}\phi_c + (4k_F - G)x], \quad (10)$$

where G is a vector of the reciprocal superlattice. The couplings g_U and K_c flow according to Eq. (2), with the replacements $g_s \rightarrow g_U$, $K_s \rightarrow K_c$ ². In the present case, however, the effective Luttinger parameter κ is a function of the transverse momentum [cf. Eq. (3)] due to the marginal interactions between wires within each array; this complicates the flow equations in the charge sector. We proceed by assuming, as a first approximation, that the flow equations for g_U and K_0 behave analogously to those in Eq. (2), in which case we naturally obtain distinct behavior at and away from half-filling: Our phase diagram in Fig. 2 indicates that, away from half-filling, the system is a SC provided K_0 is not too large; at (or near) half-filling, a large enough g_U is able to drive the system to an insulating state even for very small K_0 . Such SC-to-insulator transition is a general feature of the competing instabilities in a LL with commensurate density, because the Umklapp terms provide a “condensation” energy gain that ultimately makes the charge-gapped CDW state energetically favorable^{2,59,60}.

This competition between SC and CDW insulating states bears directly on the current experimental observations with magic-angle MTBG, which show the ground-state to be either a FL at generic densities, a SC near commensurate fillings, or an insulator at commensurability^{16,17} — the coupled LL scenario is consistent with such observation. For quantitative comparisons in this regard, it is worth noting that the electronic filling/density reported for the 2D experimental system needs to be converted to 1D electronic densities by taking into account that, in the coupled-wire picture, each Moiré unit cell contains three non-equivalent wires. For example, increasing the electron density by one electron per Moiré unit cell away from charge neutrality corresponds to adding 1/3 electrons per segment of each non-equivalent wire within that unit cell.

IV. DISCUSSION

A. Landscape of correlated states

The propagation of interacting electrons along the quantum channels provided by the well defined AB-BA domain boundaries of small-angle MTBG [Fig. 1(a)] provides a natural low-energy picture for the emergence of competing SC and insulating states. At generic densities and moderate Luttinger parameter ($|K_0| \sim 1$), we obtain SC and possibly FL as the dominant phases, with SC stabilized even for *repulsive* Coulomb interactions ($K_0 > 1$), which is noteworthy; at commensurate densities, the system is a charge-insulator. This holds both when $K_s < 1$ and $K_s > 1$, particularly in the spin-gapped regime ($K_s \gg 1$) where the only qualitative difference is the possible loss of the FL phase at very high K_s — this is significant for the model applicability to MTBG, where a magnetic field has been seen to destroy the insulating state^{16,57}.

B. Anomalous metallic behavior

Most interestingly, we see that the interaction among parallel wires contributes to stabilize both “sliding” and “crossed sliding” LL phases, thus extending previous findings for square arrays^{12–15} to this triangular geometry as well. These phases are extremely interesting because, on the one hand, they define a regime of metallic 2D transport underpinned entirely by Luttinger-liquid behavior and interactions, with the consequence that physical observables scale anomalously with temperature, size, and fields¹⁴. On the other hand, and as a result, these regimes of 2D transport are entirely different from that of an effective circuit of independent 1D wires. Perhaps most significantly for current experiments is the fact that charge transport in these phases would have anisotropic fingerprints and an anomalous temperature dependence, thus being a *natural* candidate for the “strange metal” behavior reported in magic-angle MTBG right above the temperatures where the insulating and SC states disappear⁶¹. Moreover, in this picture, a symmetry breaking among the three equivalent wire arrays would naturally impart both local and global electronic “nematicity”, a feature that has recently been inferred from high-resolution scanning tunneling microscopy (STM) experiments^{62–65}.

C. The nature of the 1D wire net

As the presence of 1D modes traveling along the AB/BA domain boundaries is a decisive precondition for modeling MTBG in terms of the proposed network of coupled Luttinger liquids, in the remainder we elaborate on their evidence so far as well as on means through which they can be ensured.

It is now well established that MTBG undergoes considerable internal deformation within each Moiré unit cell so as to maximize extension of the energetically more favorable Bernal stacking at the expense of the AA-stacked regions. This energetic tendency is constrained by frustration at the interface between AB and BA regions and results in bilayers with uniform Bernal stacking essentially everywhere, except at sharp AB/BA domain walls and AA vertices whose geometry is depicted in Fig. 1(a). Numerical calculations reveal this relaxation effect very clearly^{44–48}: it starts becoming prominent for twist angles below $\sim 2\text{--}3^\circ$ ^{47,66,67} and is completely established for $\theta \lesssim 1^\circ$, at which point the width of the domain boundaries saturates at $\sim 6\text{--}9\text{ nm}$ (becomes independent of twist amount for smaller angles)^{44,47,51}. This threshold is confirmed experimentally⁵⁵ and MTBG samples have been reported with domain walls extending up to the micron scale while retaining their atomic-scale width⁴⁴.

The electronic modes localized at the AB/BA domain boundaries of deliberately *biased* bilayer graphene are expected to behave as perfect 1D quantum wires, so long as intervalley scattering remains unimportant³⁶; explicit bandstructure calculations have recently shown this to be indeed realized in relaxed MTBL^{35,49}. More importantly, this has been confirmed by measurements that probed electric transport along isolated AB/BA boundaries extending over several microns, which revealed the expected conductance quantization at $\approx 4e^2/h$ and orders of magnitude enhancement of the mean-free path associated with these modes, when compared with that elsewhere in the sample^{50,68}. Their confinement to the domain walls has been confirmed directly by local STM and STS measurements^{51,52} as well as indirectly: (i) by the observation of Aharonov-Bohm oscillations in magnetotransport with spatial periods that correlate with closed paths along adjacent domain walls^{54,56}; (ii) by the saturation of resistance near $h/(4e^2)$ ^{55,56} and metallic temperature dependence despite increases in interlayer bias (i.e., resistivity saturation and metallic temperature dependence with increasing bulk gap)⁵⁶; (iii) and by the local enhancement of infrared optical conductivity at the AB/BA interfaces, which is associated with the presence of the 1D modes⁵³.

All of the above indicates that the coupled-wire model should provide an adequate description of biased MTBG, where the tunable bulk gap and topological character of the 1D states ensure the robustness of these electronic modes, in the regime where the Fermi level remains within the bulk gap. In the case of magic-angle MTBG, it would be interesting to experimentally investigate the fate of the correlated insulator and SC states under a finite interlayer bias.

Whether these domain-wall-bound modes survive and remain influential at zero interlayer bias can depend on the conditions of the substrate. For example: these confined modes have been seen directly by STM/STS against a gapped Bernal background of graphene bilayers deposited on graphite, without any electrostatic bias⁵¹; and

it is known that, similarly to a graphene monolayer^{37,69–72}, the Moiré and relaxation induced by boron nitride substrates generates a spectral gap for certain crystallographic orientations in bilayer graphene as well^{71,73–75}. Therefore, a bulk gap that guarantees and stabilizes the 1D modes can be engineered with appropriate substrate conditions.

Finally, we note that there is a strong pseudomagnetic field due to the lattice relaxation, with magnitudes that might exceed 10 T ^{45,66}. As a result of the triangular shape of the AB and BA domains, that field is quasi-uniform within the Bernal regions, but with opposite polarity—the polarity sharply switches precisely along the domain walls. The combined effect of large pseudomagnetic fields and abrupt polarity changes along the domain walls is likely to efficiently confine snake-type chiral states^{76,77}. These would be chiral 1D modes of a different kind, which do not require a bulk gap⁷⁶.

D. Conclusions

Different experimental probes and theoretical work are persuasive enough of the conclusion that the triangular array of coupled quantum wires illustrated in Fig. 1(a) is the natural starting point to describe transport and correlated states in biased MTBG. The accuracy of this picture increases with larger bulk gaps and angles $\lesssim 1^\circ$, which ensures the sharpest domain boundaries as well as sufficiently long channels between the AA vertices for a valid LL description of each quantum wire (the intervertex distance is 14 nm for $\theta = 1^\circ$). The facts that such modes have been equally seen in unbiased experiments and that pseudomagnetic fields can themselves beget additional 1D states of a different nature, suggest the relevance of this description to unbiased devices as well. Indeed, the phenomenology of the correlated states, which so far has been scrutinized only in the unbiased case, tallies with the phase diagram arising from the coupled LL model, namely when it comes to: the types of correlated states involved and their competition, the sequence of phase transitions with doping, the association of CDW insulating states with commensurate fillings, the existence of non-Fermi liquid metallic states, and nematicity.

Seeing as the detailed mechanisms underpinning both the insulating and SC states in MTBG remain an open problem, it is of utmost interest to experimentally scrutinize the evolution of the correlated phase diagram in MTBG (at the magic as well as smaller angles) *as a function of the bulk gap* through interlayer bias. This would place the system in the regime where our model most reliably applies, while it would also assess its relevance to the strictly unbiased case.

Note—Recently, a preprint emerged with a similar formulation⁷⁸, but with more restricted applicability directly to MTBG: it considers a wire net with C_4 symmetry rather than C_6 , assumes persistent local SC order in puddle regions that encompass the wire intersections,

and couplings are considered only at those intersections, without intra-array interactions. In specific cases (parameter ranges) where the two models can be compared, the conclusions agree.

ACKNOWLEDGMENTS

CC thanks X. Y. Gu and J. N. Leaw for helpful discussions. This work was supported by the National Research Foundation of Singapore under its Medium-Sized Centre Programme.

- * Correspondence to: vpereira@nus.edu.sg
- ¹ F. D. M. Haldane, *Journal of Physics C: Solid State Physics* **14**, 2585 (1981).
 - ² T. Giamarchi, *Quantum Physics in One Dimension* (Oxford University Press, 2003).
 - ³ E. Fradkin, *Field Theories of Condensed Matter Physics* (Cambridge University Press, 2013).
 - ⁴ J. G. Bednorz and K. A. Müller, *Zeitschrift für Physik B Condensed Matter* **64**, 189 (1986).
 - ⁵ J. M. Tranquada, D. J. Buttrey, V. Sachan, and J. E. Lorenzo, *Phys. Rev. Lett.* **73**, 1003 (1994).
 - ⁶ J. Zaanen and O. Gunnarsson, *Phys. Rev. B* **40**, 7391 (1989).
 - ⁷ K. Machida, *Phys. C Supercond.* **158**, 192 (1989).
 - ⁸ M. Kato, K. Machida, H. Nakanishi, and M. Fujita, *J. Phys. Soc. Japan* **59**, 1047 (1990).
 - ⁹ V. J. Emery, S. A. Kivelson, and J. M. Tranquada, *Proc. Natl. Acad. Sci.* **96**, 8814 (1999).
 - ¹⁰ S. P. Strong, D. G. Clarke, and P. W. Anderson, *Phys. Rev. Lett.* **73**, 1007 (1994).
 - ¹¹ X. G. Wen, *Phys. Rev. B* **42**, 6623 (1990).
 - ¹² V. J. Emery, E. Fradkin, S. A. Kivelson, and T. C. Lubensky, *Phys. Rev. Lett.* **85**, 2160 (2000).
 - ¹³ A. Vishwanath and D. Carpentier, *Phys. Rev. Lett.* **86**, 676 (2001).
 - ¹⁴ R. Mukhopadhyay, C. L. Kane, and T. C. Lubensky, *Phys. Rev. B* **63**, 081103 (2001).
 - ¹⁵ R. Mukhopadhyay, C. L. Kane, and T. C. Lubensky, *Phys. Rev. B* **64**, 045120 (2001).
 - ¹⁶ Y. Cao, V. Fatemi, A. Demir, S. Fang, S. L. Tomarken, J. Y. Luo, J. D. Sanchez-Yamagishi, K. Watanabe, T. Taniguchi, E. Kaxiras, R. C. Ashoori, and P. Jarillo-Herrero, *Nature* **556**, 80 (2018).
 - ¹⁷ Y. Cao, V. Fatemi, S. Fang, K. Watanabe, T. Taniguchi, E. Kaxiras, and P. Jarillo-Herrero, *Nature* **556**, 43 (2018).
 - ¹⁸ E. Suárez Morell, J. D. Correa, P. Vargas, M. Pacheco, and Z. Barticevic, *Phys. Rev. B* **82**, 121407 (2010).
 - ¹⁹ G. Li, A. Luican, J. M. B. Lopes dos Santos, A. H. Castro Neto, A. Reina, J. Kong, and E. Y. Andrei, *Nat. Phys.* **6**, 109 (2010).
 - ²⁰ R. Bistritzer and A. H. MacDonald, *Proc. Natl. Acad. Sci.* **108**, 12233 (2011).
 - ²¹ J. M. B. Lopes dos Santos, N. M. R. Peres, and A. H. Castro Neto, *Phys. Rev. B* **86**, 155449 (2012).
 - ²² J. M. B. Lopes dos Santos, N. M. R. Peres, and A. H. Castro Neto, *Phys. Rev. Lett.* **99**, 256802 (2007).
 - ²³ M. Koshino, N. F. Q. Yuan, T. Koretsune, M. Ochi, K. Kuroki, and L. Fu, *Phys. Rev. X* **8**, 031087 (2018).
 - ²⁴ H. C. Po, L. Zou, A. Vishwanath, and T. Senthil, *Phys. Rev. X* **8**, 031089 (2018).
 - ²⁵ J. Kang and O. Vafek, *Phys. Rev. X* **8**, 031088 (2018).
 - ²⁶ C.-C. Liu, L.-D. Zhang, W.-Q. Chen, and F. Yang, *Phys. Rev. Lett.* **121**, 217001 (2018).
 - ²⁷ H. Isobe, N. F. Q. Yuan, and L. Fu, *Phys. Rev. X* **8**, 041041 (2018).
 - ²⁸ Y.-Z. You and A. Vishwanath, *npj Quantum Materials* **4**, 16 (2019).
 - ²⁹ E. Laksono, J. N. Leaw, A. Reaves, M. Singh, X. Wang, S. Adam, and X. Gu, *Solid State Commun.* **282**, 38 (2018).
 - ³⁰ C. Xu and L. Balents, *Phys. Rev. Lett.* **121**, 087001 (2018).
 - ³¹ X. Y. Xu, K. T. Law, and P. A. Lee, *Phys. Rev. B* **98**, 121406 (2018).
 - ³² X. Gu, C. Chen, J. N. Leaw, E. Laksono, V. M. Pereira, G. Vignale, and S. Adam, arXiv e-prints, arXiv:1902.00029 (2019), arXiv:1902.00029 [cond-mat.supr-con].
 - ³³ B. Padhi, C. Setty, and P. W. Phillips, *Nano Lett.* **18**, 6175 (2018).
 - ³⁴ B. Padhi and P. W. Phillips, *Phys. Rev. B* **99**, 205141 (2019).
 - ³⁵ S. Carr, S. Fang, Z. Zhu, and E. Kaxiras, *Phys. Rev. Res.* **1**, 013001 (2019).
 - ³⁶ I. Martin, Y. M. Blanter, and A. F. Morpurgo, *Phys. Rev. Lett.* **100**, 036804 (2008).
 - ³⁷ M. Kindermann, B. Uchoa, and D. L. Miller, *Phys. Rev. B* **86**, 115415 (2012).
 - ³⁸ F. Zhang, A. H. MacDonald, and E. J. Mele, *Proc. Natl. Acad. Sci.* **110**, 10546 (2013).
 - ³⁹ A. Vaezi, Y. Liang, D. H. Ngai, L. Yang, and E.-A. Kim, *Phys. Rev. X* **3**, 021018 (2013).
 - ⁴⁰ M. Koshino, *Phys. Rev. B* **88**, 115409 (2013).
 - ⁴¹ P. San-Jose and E. Prada, *Phys. Rev. B* **88**, 121408 (2013).
 - ⁴² D. K. Efimkin and A. H. MacDonald, *Phys. Rev. B* **98**, 035404 (2018).
 - ⁴³ H. K. Pal, S. Spitz, and M. Kindermann, *Phys. Rev. Lett.* **123**, 186402 (2019).
 - ⁴⁴ J. S. Alden, A. W. Tsen, P. Y. Huang, R. Hovden, L. Brown, J. Park, D. A. Muller, and P. L. McEuen, *Proc. Natl. Acad. Sci.* **110**, 11256 (2013).
 - ⁴⁵ N. N. T. Nam and M. Koshino, *Phys. Rev. B* **96**, 075311 (2017).
 - ⁴⁶ M. Andelković, L. Covaci, and F. M. Peeters, *Phys. Rev. Mater.* **2**, 034004 (2018).
 - ⁴⁷ F. Gargiulo and O. V. Yazyev, *2D Mater.* **5**, 015019 (2017).
 - ⁴⁸ P. Lucignano, D. Alfè, V. Cataudella, D. Ninno, and G. Cantele, *Phys. Rev. B* **99**, 195419 (2019).
 - ⁴⁹ N. R. Walet and F. Guinea, *2D Mater.* **7**, 015023 (2019).
 - ⁵⁰ L. Ju, Z. Shi, N. Nair, Y. Lv, C. Jin, J. Velasco, C. Ojeda-Aristizabal, H. A. Bechtel, M. C. Martin, A. Zettl, J. Analytis, and F. Wang, *Nature* **520**, 650 (2015).
 - ⁵¹ L.-J. Yin, H. Jiang, J.-B. Qiao, and L. He, *Nat. Commun.* **7**, 11760 (2016).
 - ⁵² S. Huang, K. Kim, D. K. Efimkin, T. Lovorn, T. Taniguchi, K. Watanabe, A. H. MacDonald, E. Tutuc, and B. J. LeRoy, *Phys. Rev. Lett.* **121**, 037702 (2018).

- ⁵³ S. S. Sunku, G. X. Ni, B. Y. Jiang, H. Yoo, A. Sternbach, A. S. McLeod, T. Stauber, L. Xiong, T. Taniguchi, K. Watanabe, P. Kim, M. M. Fogler, and D. N. Basov, *Science* **362**, 1153 (2018).
- ⁵⁴ P. Rickhaus, J. Wallbank, S. Slizovskiy, R. Pisoni, H. Overweg, Y. Lee, M. Eich, M.-H. Liu, K. Watanabe, T. Taniguchi, T. Ihn, and K. Ensslin, *Nano Lett.* **18**, 6725 (2018).
- ⁵⁵ H. Yoo, R. Engelke, S. Carr, S. Fang, K. Zhang, P. Cazeaux, S. H. Sung, R. Hovden, A. W. Tsen, T. Taniguchi, K. Watanabe, G.-C. Yi, M. Kim, M. Luskin, E. B. Tadmor, E. Kaxiras, and P. Kim, *Nat. Mater.* **18**, 448 (2019).
- ⁵⁶ S. G. Xu, A. I. Berdyugin, P. Kumaravadeivel, F. Guinea, R. K. Kumar, D. A. Bandurin, S. V. Morozov, W. Kuang, B. Tsim, S. Liu, J. H. Edgar, I. V. Grigorieva, V. I. Fal'ko, M. Kim, and A. K. Geim, *Nat. Commun.* **10**, 4008 (2019).
- ⁵⁷ M. Yankowitz, S. Chen, H. Polshyn, Y. Zhang, K. Watanabe, T. Taniguchi, D. Graf, A. F. Young, and C. R. Dean, *Science* **363**, 1059 (2019).
- ⁵⁸ X.-C. Wu, C.-M. Jian, and C. Xu, *Phys. Rev. B* **99**, 161405 (2019).
- ⁵⁹ T. Giamarchi, *Physica B: Condensed Matter* **230-232**, 975 (1997), proceedings of the International Conference on Strongly Correlated Electron Systems.
- ⁶⁰ V. J. Emery, "Theory of the one-dimensional electron gas," in *Highly Conducting One-Dimensional Solids*, edited by J. T. Devreese, R. P. Evrard, and V. E. van Doren (Springer US, Boston, MA, 1979) pp. 247–303.
- ⁶¹ Y. Cao, D. Chowdhury, D. Rodan-Legrain, O. Rubies-Bigordà, K. Watanabe, T. Taniguchi, T. Senthil, and P. Jarillo-Herrero, arXiv preprint (2019), [1901.03710](https://arxiv.org/abs/1901.03710).
- ⁶² Y. Jiang, X. Lai, K. Watanabe, T. Taniguchi, K. Haule, J. Mao, and E. Y. Andrei, *Nature* (2019), [10.1038/s41586-019-1460-4](https://doi.org/10.1038/s41586-019-1460-4), [1904.10153](https://doi.org/10.1038/s41586-019-1460-4).
- ⁶³ A. Kerelsky, L. J. McGilly, D. M. Kennes, L. Xian, M. Yankowitz, S. Chen, K. Watanabe, T. Taniguchi, J. Hone, C. Dean, A. Rubio, and A. N. Pasupathy, *Nature* **572**, 95 (2019).
- ⁶⁴ Y. Choi, J. Kemmer, Y. Peng, A. Thomson, H. Arora, R. Polski, Y. Zhang, H. Ren, J. Alicea, G. Refael, F. von Oppen, K. Watanabe, T. Taniguchi, and S. Nadj-Perge, *Nat. Phys.* (2019), [10.1038/s41567-019-0606-5](https://doi.org/10.1038/s41567-019-0606-5).
- ⁶⁵ Y. Xie, B. Lian, B. Jäck, X. Liu, C.-I. Chiu, K. Watanabe, T. Taniguchi, B. A. Bernevig, and A. Yazdani, *Nature* **572**, 101 (2019).
- ⁶⁶ M. M. van Wijk, A. Schuring, M. I. Katsnelson, and A. Fasolino, *2D Mater.* **2**, 034010 (2015).
- ⁶⁷ K. Zhang and E. B. Tadmor, *J. Mech. Phys. Solids* **112**, 225 (2018).
- ⁶⁸ J. Li, K. Wang, K. J. McFaul, Z. Zern, Y. Ren, K. Watanabe, T. Taniguchi, Z. Qiao, and J. Zhu, *Nat. Nanotechnol.* **11**, 1060 (2016).
- ⁶⁹ B. Hunt, J. D. Sanchez-Yamagishi, A. F. Young, M. Yankowitz, B. J. LeRoy, K. Watanabe, T. Taniguchi, P. Moon, M. Koshino, P. Jarillo-Herrero, and R. C. Ashoori, *Science* **340**, 1427 (2013).
- ⁷⁰ Z.-G. Chen, Z. Shi, W. Yang, X. Lu, Y. Lai, H. Yan, F. Wang, G. Zhang, and Z. Li, *Nat. Commun.* **5**, 4461 (2014).
- ⁷¹ P. Moon and M. Koshino, *Phys. Rev. B* **90**, 155406 (2014).
- ⁷² J. Jung, A. M. DaSilva, A. H. MacDonald, and S. Adam, *Nat. Commun.* **6**, 6308 (2015).
- ⁷³ M. Mucha-Kruczynski, J. R. Wallbank, and V. I. Fal'ko, *Phys. Rev. B* **88** (2013), [10.1103/PhysRevB.88.205418](https://doi.org/10.1103/PhysRevB.88.205418).
- ⁷⁴ C. R. Dean, L. Wang, P. Maher, C. Forsythe, F. Ghahari, Y. Gao, J. Katoch, M. Ishigami, P. Moon, M. Koshino, T. Taniguchi, K. Watanabe, K. L. Shepard, J. Hone, and P. Kim, *Nature* **497**, 598 (2013).
- ⁷⁵ H. Kim, N. Leconte, B. L. Chittari, K. Watanabe, T. Taniguchi, A. H. MacDonald, J. Jung, and S. Jung, *Nano Lett.* **18**, 7732 (2018).
- ⁷⁶ G. W. Jones, D. A. Bahamon, A. H. Castro Neto, and V. M. Pereira, *Nano Lett.* **17**, 5304 (2017).
- ⁷⁷ J. E. Müller, *Phys. Rev. Lett.* **68**, 385 (1992).
- ⁷⁸ Y.-Z. Chou, Y.-P. Lin, S. Das Sarma, and R. M. Nandkishore, *Phys. Rev. B* **100**, 115128 (2019).

Appendix A: Bosonization conventions

According to the bosonization approach^{2,3}, the fermion field from the l -th wire of array j with spin σ and direction μ (+1 for right and -1 for left) reads

$$\psi_{l,\mu,\sigma}^j \propto \frac{1}{\sqrt{2\pi\alpha}} e^{i\mu 2\sqrt{\pi}\phi_{l,\mu,\sigma}^j}, \quad (\text{A1})$$

where α is the length cut-off. The bosonic fields are related by:

$$\phi_{l,\sigma}^j = \phi_{l,+,\sigma}^j + \phi_{l,-,\sigma}^j, \quad (\text{A2a})$$

$$\theta_{l,\sigma}^j = -\phi_{l,+,\sigma}^j + \phi_{l,-,\sigma}^j, \quad (\text{A2b})$$

$$\phi_{l,c/s}^j = \frac{1}{\sqrt{2}}(\phi_{l,\uparrow}^j \pm \phi_{l,\downarrow}^j), \quad (\text{A2c})$$

$$\theta_{l,c/s}^j = \frac{1}{\sqrt{2}}(\theta_{l,\uparrow}^j \pm \theta_{l,\downarrow}^j). \quad (\text{A2d})$$

The subscript c/s in Eq. (A2)(c,d) stands for the charge/spin sector. The bosonic fields are related to the electron densities through:

$$\frac{1}{\sqrt{\pi}} \partial_{x_j} \phi_{l,\mu,\sigma}^j = \rho_{l,\mu,\sigma}^j, \quad (\text{A3a})$$

$$\frac{1}{\sqrt{\pi}} \partial_{x_j} \phi_{l,c/s}^j = \frac{1}{\sqrt{2}} (\rho_{l,+c/s}^j + \rho_{l,-c/s}^j), \quad (\text{A3b})$$

$$\frac{1}{\sqrt{\pi}} \partial_{x_j} \theta_{l,c/s}^j = \frac{1}{\sqrt{2}} (-\rho_{l,+c/s}^j + \rho_{l,-c/s}^j), \quad (\text{A3c})$$

where x_j is the variable along the direction of j -th array and $\rho_{c/s}$ stands for the charge/spin density, i.e., $\rho_{c/s} = \rho_{\uparrow} \pm \rho_{\downarrow}$.

Appendix B: Bosonized form of the couplings

Once we know the bosonized form of the fermion fields, it is straightforward to write all the couplings in terms of the bosonic fields defined in the previous section. For the intra-array couplings, we consider an array of parallel wires along the x direction [see the schematic of array-1 in Fig. 1(a) as an example]: The Hamiltonian terms describing the coupling between wires separated by a distance nd are:

$$\begin{aligned} H_{c,n}^j &= \mathcal{V}_n \sum_l \sum_{\mu,\sigma,\sigma'} \int dx \psi_{l,\mu,\sigma}^{j,\dagger} \psi_{l,-\mu,\sigma}^j \psi_{l+n,-\mu,\sigma'}^{j,\dagger} \psi_{l+n,\mu,\sigma'}^j \\ &= \frac{2\mathcal{V}_n}{(\pi\alpha)^2} \sum_l \int dx \cos \left[\sqrt{2\pi} (\phi_{l,c}^j - \phi_{l+n,c}^j) \right] \cos(\sqrt{2\pi} \phi_{l,s}^j) \cos(\sqrt{2\pi} \phi_{l+n,s}^j) \end{aligned} \quad (\text{B1a})$$

$$\begin{aligned} H_{sc,n}^j &= \mathcal{J}_n \sum_{l,\mu,\nu} \int dx \psi_{l,\mu,\uparrow}^{j,\dagger} \psi_{l,-\mu,\downarrow}^{j,\dagger} \psi_{l+n,\nu,\downarrow}^j \psi_{l+n,-\nu,\uparrow}^j + \text{H. c.} \\ &= \frac{2\mathcal{J}_n}{(\pi\alpha)^2} \sum_l \int dx \cos \left[\sqrt{2\pi} (\theta_{l,c}^j - \theta_{l+n,c}^j) \right] \cos(\sqrt{2\pi} \phi_{l,s}^j) \cos(\sqrt{2\pi} \phi_{l+n,s}^j) \end{aligned} \quad (\text{B1b})$$

$$\begin{aligned} H_h^j &= t_{\perp} \sum_l \sum_{\mu,\sigma} \int dx \psi_{l,\mu,\sigma}^{j,\dagger} \psi_{l+1,\mu,\sigma}^j + \text{H. c.} \\ &= \frac{2t_{\perp}}{\pi\alpha} \sum_l \int dx \cos \left[\sqrt{\frac{\pi}{2}} (\phi_{l,c}^j - \theta_{l,c}^j - \phi_{l+1,c}^j + \theta_{l+1,c}^j) \right] \cos \left[\sqrt{\frac{\pi}{2}} (\phi_{l,s}^j - \theta_{l,s}^j - \phi_{l+1,s}^j + \theta_{l+1,s}^j) \right] \\ &\quad \times \cos \left[\sqrt{\frac{\pi}{2}} (\phi_{l,c}^j + \theta_{l,c}^j - \phi_{l+1,c}^j - \theta_{l+1,c}^j) \right] \cos \left[\sqrt{\frac{\pi}{2}} (\phi_{l,s}^j + \theta_{l,s}^j - \phi_{l+1,s}^j - \theta_{l+1,s}^j) \right] \end{aligned} \quad (\text{B1c})$$

Meanwhile, the inter-array couplings at a crossing point (e.g., the intersection of the l -th wire from array k and the m -th from array j) can be written in the form:

$$\begin{aligned} H_{cdw}^{k,j} &= \mathcal{V}_0 \sum_{\mu,\nu,\sigma,\sigma'} \psi_{l,\mu,\sigma}^{k\dagger} \psi_{l,-\mu,\sigma}^k \psi_{m,\nu,\sigma'}^{j\dagger} \psi_{m,-\nu,\sigma'}^j \\ &= \frac{4\mathcal{V}_0}{(\pi\alpha)^2} \cos(\sqrt{2\pi}\phi_{l,c}^k) \cos(\sqrt{2\pi}\phi_{l,s}^k) \cos(\sqrt{2\pi}\phi_{m,c}^j) \cos(\sqrt{2\pi}\phi_{m,s}^j) \end{aligned} \quad (\text{B2a})$$

$$\begin{aligned} H_{sc}^{k,j} &= \mathcal{J}_0 \sum_{\mu,\nu} \psi_{l,\mu,\uparrow}^{k\dagger} \psi_{l,-\mu,\downarrow}^{k\dagger} \psi_{m,\nu,\downarrow}^j \psi_{m,-\nu,\uparrow}^j + \text{H. c.} \\ &= \frac{4\mathcal{J}_0}{(\pi\alpha)^2} e^{i\sqrt{2\pi}(\theta_{l,c}^k - \theta_{m,c}^j)} \cos(\sqrt{2\pi}\phi_{l,s}^k) \cos(\sqrt{2\pi}\phi_{m,s}^j) + \text{H. c.} \end{aligned} \quad (\text{B2b})$$

$$\begin{aligned} H_h^{k,j} &= t \sum_{\mu,\nu,\sigma} \psi_{l,\mu,\sigma}^{k\dagger} \psi_{m,\nu,\sigma}^j + \text{H. c.} \\ &= \frac{t}{\pi\alpha} \sum_{\sigma} e^{i\sqrt{\frac{\pi}{2}}(\theta_{l,c}^k + \sigma\theta_{l,s}^k - \theta_{m,c}^j - \sigma\theta_{m,s}^j)} \cos\left[\sqrt{\frac{\pi}{2}}(\phi_{l,c}^k + \sigma\phi_{l,s}^k)\right] \cos\left[\sqrt{\frac{\pi}{2}}(\phi_{m,c}^j + \sigma\phi_{m,s}^j)\right] + \text{H. c.} \end{aligned} \quad (\text{B2c})$$

Having obtained the identities above, one can proceed with the perturbative RG calculation to explore the potential instabilities of the system.
